

# Colonic epithelial response to injury requires Myd88 signaling in myeloid cells

NP Malvin<sup>1,2</sup>, H Seno<sup>1,2</sup> and TS Stappenbeck<sup>1</sup>

Proper colonic injury response requires myeloid-derived cells and Toll-like receptor/Myd88 signaling. However, the precise role of Myd88 signaling specifically in myeloid-derived cells that occurs during tissue damage is unclear. Therefore, we created a mouse line with Myd88 expression restricted to myeloid lineages (*Myd88*<sup>-/-</sup>; *LysM*<sup>Cre/+</sup>; *ROSA26*<sup>Myd88/+</sup>; herein *Mlcr*). In these mice, Myd88 was appropriately expressed and mediated responses to bacterial ligand exposure in targeted cells. Importantly, the severe colonic epithelial phenotype observed in dextran sodium sulfate-injured *Myd88*<sup>-/-</sup> mice was rescued by the genetic modification of *Mlcr* mice. During injury, myeloid cell activation and enrichment of Ptsg2-expressing stromal cells occurred within the mesenchyme that surrounded the crypt bases of *Mlcr* and *Myd88*<sup>+/-</sup> mice but not *Myd88*<sup>-/-</sup> mice. Interestingly, these cellular changes to the crypt base mesenchyme also occurred, but to a lesser extent in uninjured *Mlcr* mice. These results show that Myd88 expression in myeloid cells was sufficient to rescue intestinal injury responses, and surprisingly, these cells appear to require an additional Myd88-dependent signal from a non-myeloid cell type during homeostasis.

## INTRODUCTION

The mouse colon is a distinctive model system that can be utilized to elucidate functional cellular components that mediate damage responses. The epithelium is an absorptive barrier composed of a single layer of cells lining the inner surface of the colonic tube. The apical side of this barrier contacts a substantial and diverse set of indigenous microbes while the basal side contacts cells of the immune system and the stroma.<sup>1–3</sup> Studies of colonic wound responses and repair suggest this process requires interaction with both the apically located microbes and the baso-laterally located cells of the innate immune system and stroma.<sup>4</sup>

The mouse colonic epithelium is designed to quickly respond to injury. Cellular turnover is already quite elevated during homeostasis (~3–5 days). New epithelial cells are supplied from ~100,000 crypts that are organized in a high-density array (~400 crypts mm<sup>-2</sup>). Stem and proliferative progenitors are located at the base of each crypt.<sup>5,6</sup> Their daughters exit the cell cycle, and migrate upwards and eventually out of crypts onto the inner surface of the intestine. To properly respond to injury, stem and progenitor cells alter their activity to repopulate damaged crypts and the epithelial barrier.<sup>7</sup>

Interaction of the epithelium with mesenchymal cells is critical for proper injury response.<sup>8,9</sup> In the colon, a number

of cell types have been proposed to have a role in injury repair using a variety of experimental systems.<sup>2,3</sup> Myeloid cells are often a prominent cell type within areas of intestinal damage, and engage in an important function of killing and clearing microbes. Under certain circumstances, these cells appear to have a role in the proper response to injury. For example, in the intestine, mice with greatly diminished peripheral myeloid cells (*Csf1*<sup>op/op</sup> mice) when injured with the toxin dextran sodium sulfate (DSS) show loss of proliferation in colonic epithelial progenitors supporting a positive role for myeloid cells in the response to tissue injury.<sup>10,11</sup> Elimination of myeloid cells using the inducible diphtheria toxin receptor model showed that these cells have a role in specific phases of skin wound healing.<sup>12</sup>

Toll-like receptor (TLR) signaling through the Myd88 adaptor protein is a critical signaling pathway required for proper colonic injury response to DSS.<sup>13,14</sup> This signaling is responsible for microbial recognition, induction of antimicrobial products, and modulation of the adaptive immune response.<sup>15,16</sup> TLRs are key recognition molecules within the colon, functioning within many specialized cells, potentially including epithelial cells, myofibroblasts, and professional immune cells.<sup>17,18</sup>

We previously found that Myd88 signaling was upstream of focal prostaglandin E2 (PGE2) production during DSS

<sup>1</sup>Department of Pathology and Immunology, Washington University School of Medicine, St Louis, Missouri, USA. <sup>2</sup>These authors contributed equally to this work. Correspondence: TS Stappenbeck (stappenb@pathology.wustl.edu)

Received 3 August 2011; accepted 5 December 2011; published online 18 January 2012. doi:10.1038/mi.2011.65

injury.<sup>13</sup> A rate-limiting enzyme for the production of PGE2 is Pts2 (also known as Cox-2).<sup>19</sup> We and others have found that this gene is highly expressed in a population of non-hematopoietic cells in the stroma of the mouse colon,<sup>13,20</sup> and that *in vitro* these cells are consistent with mesenchymal stem cells.<sup>21</sup> In non-ulcerated areas of DSS damage in the mouse rectum, we found that the positioning of the Pts2-expressing stromal cells (PSCs) was important to maintain colonic epithelial proliferation during this injury.<sup>13</sup> We proposed that the position of these cells was important because PGE2 has a very short half-life and its delivery closer to intestinal epithelial progenitors that are its target would increase its effects.<sup>22</sup> PGE2 has been proposed to stimulate Wnt signaling, which is required for intestinal epithelial progenitor function during injury.<sup>23</sup>

Our model is that to maintain colonic epithelial proliferation during DSS injury, Myd88 signaling is required in a lineage distinct from the PSCs. One reason is that the latter cell type does not respond to TLR ligands, such as lipopolysaccharide (LPS), as they lack CD14 expression.<sup>21</sup> Based on our findings with *Csf1<sup>op/op</sup>* mice,<sup>10</sup> we developed the hypothesis that Myd88 signaling was required in myeloid cells for the proper response to DSS damage. To test this hypothesis, we created a novel mouse line with Myd88 expression that was restricted to these cells. Here, we show that our targeting strategy produced appropriate expression of Myd88 in myeloid cells and that this expression was sufficient to rescue the phenotype observed in DSS-injured *Myd88<sup>-/-</sup>* mice.

## RESULTS

### Generation and validation of the *Mlcr* mouse strain

We engineered a mouse line that contained Myd88 expression in myeloid-derived cells. We “knocked in” the Myd88 complementary DNA (cDNA) into the *Rosa26* locus immediately downstream of its floxed stop signal (Figure 1a–c).<sup>24–26</sup> *ROSA26<sup>Myd88/+</sup>* mice were bred to *Myd88<sup>-/-</sup>* and their progeny were then bred to *LysM<sup>Cre/Cre</sup>* mice. We used this Cre line as recombination has been widely reported to occur in myeloid lineages, including macrophages, GR-1<sup>+</sup> leukocytes, and dendritic cells.<sup>27,28</sup> The breeding scheme generated *Mlcr* mice (*Myd88<sup>-/-</sup>;LysM<sup>Cre/+</sup>*; and *ROSA26<sup>Myd88/+</sup>*) as well as two littermate control groups: *Myd88<sup>+/-</sup>;LysM<sup>Cre/+</sup>*; and *ROSA26<sup>+/+</sup>* (herein *Myd88<sup>+/-</sup>*) and *Myd88<sup>-/-</sup>;LysM<sup>Cre/+</sup>*; and *ROSA26<sup>+/+</sup>* (herein *Myd88<sup>-/-</sup>*). We generated *Myd88<sup>+/-</sup>* mice as controls as mice with this genotype have been shown to be functionally equivalent to *Myd88<sup>+/+</sup>* mice.<sup>29</sup> Using breeding scheme one (generated *Mlcr*, *Myd88<sup>-/-</sup>*, and *Myd88<sup>+/-</sup>* mice), we found that the distribution of mice obtained was not significantly different than the expected Mendelian ratio (Table 1). Using breeding scheme two (generated *Mlcr* and *Myd88<sup>-/-</sup>* mice), we found that *Mlcr* mice were present at ratios significantly higher than the expected Mendelian frequencies (Table 1).

To validate the genetic targeting, we determined the level of Myd88 expression in myeloid cells and fibroblasts isolated from colons of *Mlcr* and control mice (*Myd88<sup>+/-</sup>* and

*Myd88<sup>-/-</sup>*). We isolated an enriched population of colonic myeloid cells (<95% F4/80 positive) using a protocol based on multiple previous studies<sup>30–33</sup> (Supplementary Figure S1 online). Using quantitative real-time PCR analysis, Myd88 expression was at the limit of detection in myeloid cells isolated from *Myd88<sup>-/-</sup>* mice and was detectable at comparable levels in cells isolated from *Mlcr* and *Myd88<sup>+/-</sup>* mice (Figure 2a). To confirm the specificity of *LysM-Cre* in the *Mlcr* mice, we evaluated Myd88 messenger RNA (mRNA) expression in colonic fibroblasts isolated as previously described.<sup>21</sup> Myd88 expression was at the limit of detection in fibroblasts isolated from *Mlcr* and *Myd88<sup>-/-</sup>* mice, and was detectable in cells isolated from *Myd88<sup>+/-</sup>* mice (Figure 2b). We confirmed in separate experiments that *Myd88<sup>+/+</sup>* and *Myd88<sup>+/-</sup>* mice from our colony expressed similar levels of Myd88 mRNA (Supplementary Figure S2 online). We also performed immunofluorescence localization of Myd88 on colonic sections using tyramide amplification. By this method, we detected Myd88 in the crypt epithelium of *Myd88<sup>+/+</sup>* and *Myd88<sup>+/-</sup>* mice but not in the epithelium of *Mlcr* and *Myd88<sup>-/-</sup>* mice (Supplementary Figure S3 online). Thus, constitutive expression of Myd88 mRNA occurred as expected based on the known cellular targets of *LysM-Cre*.

### Myeloid cells in *Mlcr* mice have functional expression of Myd88

To perform functional tests of Myd88 expression in *Mlcr* mice, we isolated bone marrow monocytes and performed *in vitro* differentiation for macrophages (M-CSF) and dendritic cells (GM-CSF),<sup>34</sup> and confirmed appropriate expression of Myd88. We chose this model as both of these cell populations are readily expanded *in vitro*. As expected, Myd88 expression in macrophages and dendritic cells derived from *Myd88<sup>-/-</sup>* mice was at the limits of detection. *Myd88<sup>+/-</sup>* and *Mlcr* mice expressed comparable levels of Myd88 mRNA in bone marrow-derived macrophages (Figure 3a). As an additional control, we found the levels of Myd88 expression were similar in *Myd88<sup>+/-</sup>* and *Myd88<sup>+/+</sup>* bone marrow-derived macrophages (Supplementary Figure S4a online). The levels of Myd88 expression in dendritic cells from *Mlcr* mice were 1.6-fold less than those isolated from *Myd88<sup>+/-</sup>*.

As Myd88 expression is critical to drive responses to bacterial products,<sup>14–16</sup> we treated bone marrow-derived macrophages and dendritic cells from *Mlcr* and control mice with LPS, and evaluated gene expression of two well-known targets, Pts2 and tumor necrosis factor (TNF)- $\alpha$ .<sup>15,21</sup> At baseline, gene expression for both Pts2 and TNF- $\alpha$  showed no significant differences based on genotype for both macrophages and dendritic cells (Figure 3b and c; Supplementary Figure S4b, c online). LPS-treated macrophages and dendritic cells from *Myd88<sup>+/-</sup>* and *Mlcr* mice expressed higher levels of Pts2 and TNF- $\alpha$  as compared with corresponding LPS-treated *Myd88<sup>-/-</sup>* cells (Figure 3d and e; Supplementary Figure S4b, c online). Taken together, these results were consistent with functional levels of Myd88 expression in myeloid cells isolated from *Mlcr* mice.

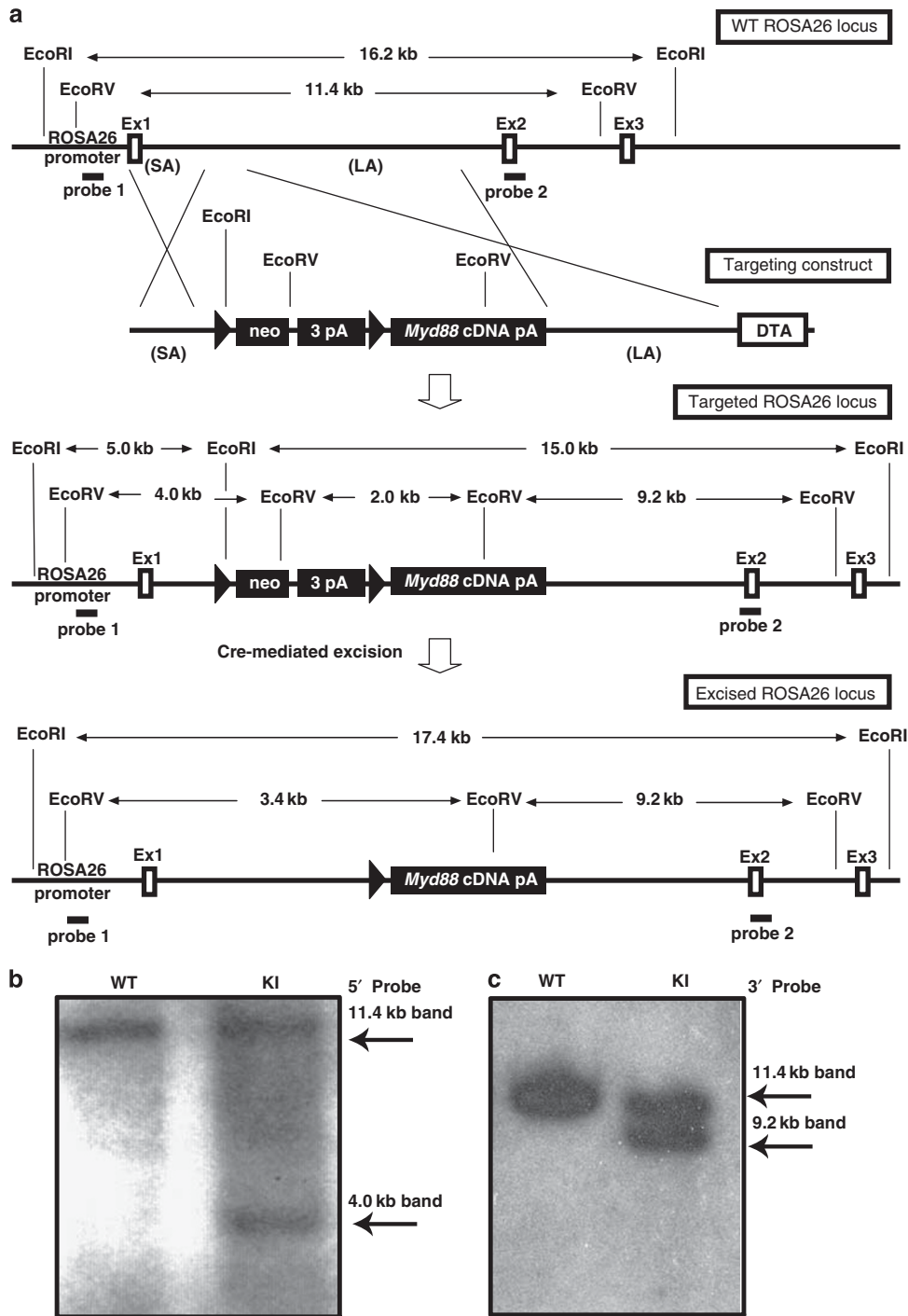


**Figure 1** Generation of *Mlcr* mice. (a) Targeting of *Myd88* complementary DNA (cDNA) into the ROSA26 locus. The targeting construct included two homology arms indicated as SA (the “short arm” at the 5’ position of the targeting construct) and LA (the “long arm” at the 3’ position), the *Myd88* cDNA, as well as two flox sites (denoted by filled triangles) that flank the neomycin resistance gene plus its three tandem polyadenylation sites (3 pA). The map indicates proper targeting of the construct into the ROSA26 locus by homologous recombination as well as the predicted effects of Cre-mediated excision on a properly targeted locus. *EcoRV* digestion of genomic DNA was used to map clones, and anticipated sizes of DNA fragments were indicated. (b, c) Southern blots showed clones that are either not targeted (wild-type (WT)) or properly targeted (knocked in) using (b) 5’ and (c) 3’ probes. The targeted ROSA26 locus contained a 4.0-kb *EcoRV* DNA fragment recognized by probe1 and a 9.2-kb *EcoRV* DNA fragment recognized by probe 2.

**Myeloid expression of *Myd88* rescues the DSS injury phenotype of *Myd88*<sup>-/-</sup> mice**

We next evaluated the colonic damage response of adult mice treated for 1 week with 2.5% DSS. This experimental treatment

created multiple focal ulcers in the transverse colon as well as a single confluent ulcer at the ano-rectal junction in *Mlcr* mice as well as their littermate controls. Importantly, the descending colons of DSS-treated *Mlcr* mice and controls were neither

**Table 1** *Mlcr* mice exhibited improved survival as compared with *Myd88*<sup>-/-</sup> littermates

Breeding scheme	Parents	<i>Myd88</i>	<i>LysM</i> <sup>Cre/+</sup>	<i>Rosa26R</i> <sup><i>Myd88</i>+/+</sup>
1	♂	+/-	+/-	+/-
	♀	-/-	+/-	+/-
2	♂	-/-	+/-	+/-
	♀	-/-	+/-	+/-

Breeding scheme 1	<i>Myd88</i> <sup>-/-</sup>	<i>Mlcr</i>	<i>Myd88</i> <sup>+/-</sup>
Total mice	14	27	39
Actual (%)	17	34	49
Expected (Mendelian) (%)	22	28	50

Breeding scheme 2	<i>Myd88</i> <sup>-/-</sup>	<i>Mlcr</i>	<i>Myd88</i> <sup>+/-</sup>
Total mice	21	59	NA
Actual (%)	26*	74*	
Expected (Mendelian) (%)	44	56	

Abbreviation: NA, not applicable.

Survival table of actual vs. expected birthrates for the two breeding schemes used to generate littermate controls. Asterisks indicate a statistically significant difference between groups (\* $P < 0.05$ ,  $\chi^2$  test).

ulcerated nor inflamed as evidenced by the absence of accumulated mucosal neutrophils in this location for any group of DSS-treated mice (**Supplementary Figure S5** online). These findings were similar to previous studies with DSS-treated mice.<sup>10,13</sup>

We next performed histological analysis of descending colons from groups of untreated and DSS-treated mice. The descending colon of untreated *Mlcr* mice was similar in appearance to untreated colons from *Myd88*<sup>+/-</sup> and *Myd88*<sup>-/-</sup> mice (**Figure 4a–c**). We found no discernable differences when comparing untreated and DSS-treated *Myd88*<sup>+/-</sup> mice (**Figure 4a** and **d**). In contrast, DSS-treated *Myd88*<sup>-/-</sup> mice contained extensive crypt atrophy, loss of crypt epithelial cells, and a thickened muscularis propria as compared with untreated *Myd88*<sup>-/-</sup> mice (**Figure 4b** and **e**). Interestingly, the descending colons from DSS-treated *Mlcr* mice showed no apparent differences in comparison with untreated *Mlcr* mice (**Figure 4c** and **f**). These results showed that expression of *Myd88* in myeloid cells rescued the effects of DSS injury in *Myd88*<sup>-/-</sup> mice. *LysM* targets multiple myeloid cell types including macrophages, dendritic cells, and neutrophils.<sup>27,28</sup> We found that ablation of neutrophils in wild-type mice did not alter the epithelial response to DSS treatment, suggesting this cell type is not required (**Supplementary Figure S6** online).

As the descending colonic crypts were a primary morphological target of DSS in *Myd88*<sup>-/-</sup> mice, we qualitatively evaluated crypt size by H + E staining and epithelial proliferation by 5-bromo-2-deoxyuridine incorporation to visualize cells in S-phase (**Figure 5a–f**). These stained sections showed that

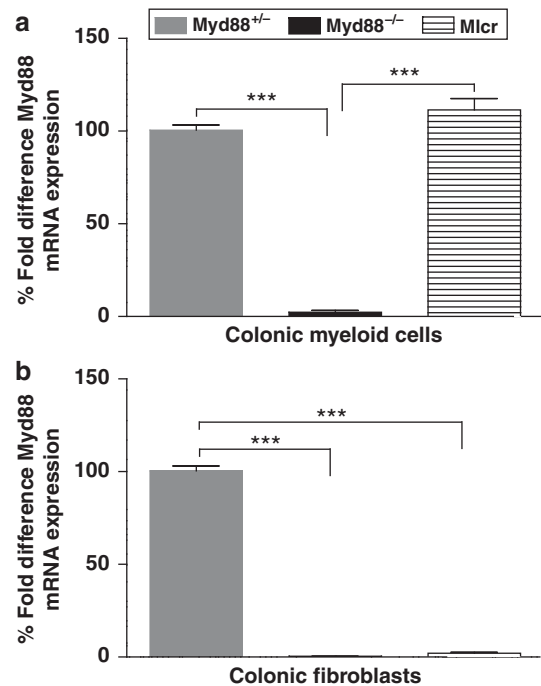


**Figure 2** *Mlcr* mice expressed *Myd88* messenger RNA (mRNA) in colonic isolated myeloid cells. Graphs of the percentage fold difference of *Myd88* mRNA expression of isolated colonic cell populations. (a) Isolated colonic myeloid cells. (b) Isolated colonic fibroblasts. For each cell type, Y-axis values were calculated as percentage of a fold difference of *Myd88* mRNA expression by quantitative real-time PCR analysis. The fold difference was calculated as the difference between the average  $\Delta C_T$  of the experimental cell type and average  $\Delta C_T$  of the control cells (untreated *Myd88*<sup>+/-</sup>) divided by the control  $\Delta C_T$ . Mean values  $\pm$  s.e.m. were plotted for each group ( $N = 4$ – $6$  samples per group performed in two separate experiments). Triple asterisks indicate a statistically significant difference between two groups ( $P < 0.001$ ) as determined by a one-way analysis of variance with a Tukey's post-test.

crypts from DSS-treated *Myd88*<sup>-/-</sup> mice contained fewer total and S-phase cells as compared with all other groups of mice. We next performed quantitative analysis of epithelial proliferation, cell census, and cell death of the intestinal epithelium in DSS-treated and untreated mice (**Figure 5g–j**). Quantification of total numbers of epithelial cells/crypt, M-phase cells/crypt, and S-phase cells/crypt showed that DSS-treated *Myd88*<sup>-/-</sup> mice had a significant reduction in cell census and proliferation as compared with untreated *Myd88*<sup>-/-</sup> mice (**Figure 5g–i**). These differences were present for all the genetic subgroups of *Myd88*<sup>-/-</sup> mice obtained by our breeding scheme (**Supplementary Figure S7** online). Importantly, we found that DSS-treated *Mlcr* mice showed no reduction in epithelial cell census and proliferation compared with untreated *Mlcr* mice (**Figure 5g–i**). The findings for DSS-treated *Mlcr* mice were comparable to similarly treated *Myd88*<sup>+/-</sup> controls (including subgroups of *Myd88*<sup>+/-</sup>, **Supplementary Figure S7** online). Quantification of apoptosis was determined by visualization of apoptotic bodies in the epithelium.<sup>10,13</sup> This analysis showed no significant differences when comparing DSS-treated and untreated mice for all three genotypes (**Figure 5j**).

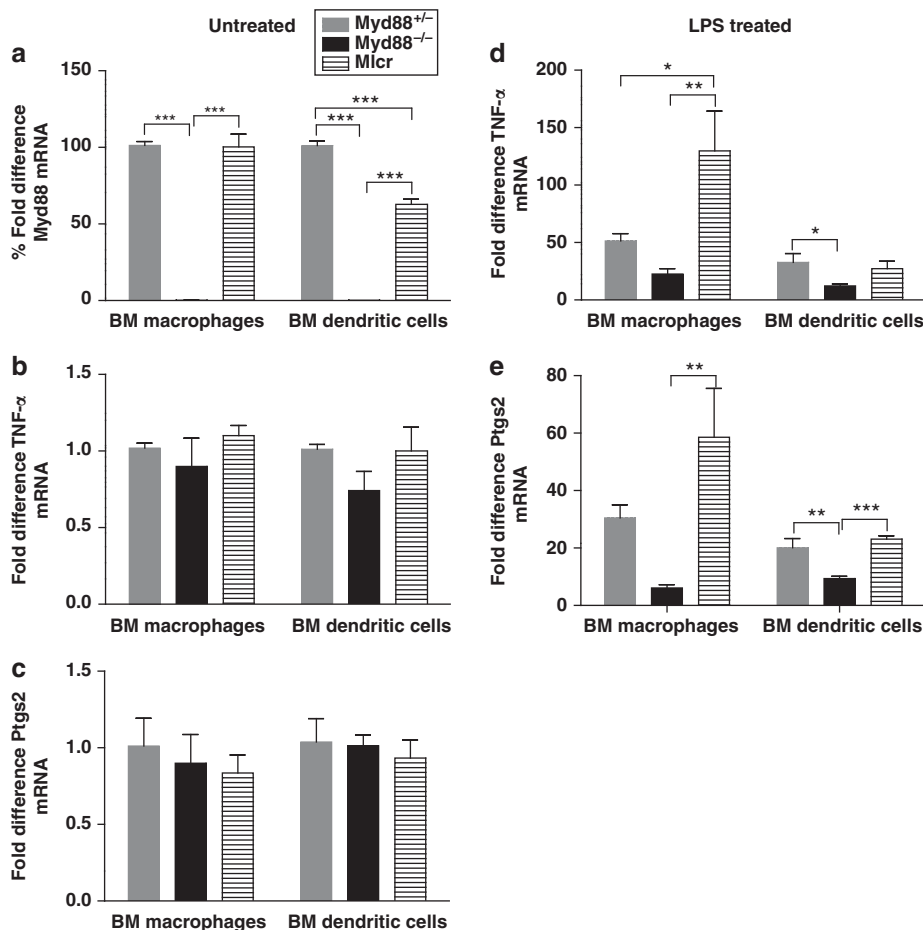


**Figure 3** Bone marrow (BM)-derived macrophages and dendritic cells from *Mlcr* mice showed elevated *Ptgs2* and tumor necrosis factor (TNF)- $\alpha$  production in response to lipopolysaccharide (LPS) treatment. **(a)** Graphs of the percentage fold difference of *Myd88* messenger RNA (mRNA) expression in BM-derived macrophages and dendritic cells. For each cell type, Y-axis values were calculated as percentage of a fold difference of *Myd88* mRNA expression by quantitative real-time PCR analysis. The fold difference was calculated as the difference between the average  $\Delta C_T$  of the experimental cell type and average  $\Delta C_T$  of the control cells (untreated *Myd88*<sup>+/-</sup>) divided by the control  $\Delta C_T$ . **(b–e)** Graphs of the relative mRNA expression levels of **(b, d)** TNF- $\alpha$  and **(c, e)** *Ptgs2* in BM-derived macrophages and dendritic cells. Cells were either **(b, c)** untreated or **(d, e)** treated with 10 ng of LPS for 1 h. For each cell type, Y-axis values were a fold difference between the average  $\Delta C_T$  of the experimental cell type and average  $\Delta C_T$  of the control cells (untreated *Myd88*<sup>+/-</sup>) divided by the control  $\Delta C_T$ . Mean values  $\pm$  s.e.m. were plotted for each group ( $N=9$ –12 samples per group performed in 2–3 separate experiments). Asterisks indicate a statistically significant difference between two indicated groups (\* $P<0.05$ , \*\* $P<0.01$ , \*\*\* $P<0.001$ ) as determined by a one-way analysis of variance and Tukey's post-test.

### *Mlcr* mice contain activated colonic myeloid cells during DSS injury

We previously found that based on morphology, activated myeloid cells were present in the peri-crypt base mesenchyme of DSS-treated wild-type but not similarly treated *Myd88*<sup>-/-</sup> mice.<sup>10</sup> To test if *Myd88* expression within myeloid cells stimulated activation during injury, we analyzed slides co-labeled with antisera directed against F4/80 and CD86. The latter is a recently established marker of macrophage activation.<sup>35–38</sup> In mice of all three genotypes, CD86-positive aggregates were preferentially located in the crypt base-associated mesenchyme and often co-localized with F4/80 (**Figure 6a** and **b**). Quantification of the number of double-positive aggregates (CD86 and F4/80) per crypt-associated mesenchyme showed significantly higher numbers in DSS-treated *Myd88*<sup>+/-</sup> and *Mlcr* mice as compared with untreated genotype controls (**Figure 6c**). As an additional

control, the numbers of double-positive aggregates were similar in DSS-treated and untreated *Myd88*<sup>+/-</sup> and *Myd88*<sup>+/+</sup> (**Supplementary Figure S8** online). In contrast, the number of double-positive aggregates was not significantly increased in DSS-treated vs. untreated *Myd88*<sup>-/-</sup> mice (**Figure 6c**). As an additional control, we found that nearly all of the CD86-positive aggregates co-localized with F4/80 in DSS-treated *Myd88*<sup>+/-</sup>, *Myd88*<sup>+/+</sup>, and *Mlcr* mice (**Figure 6d**; **Supplementary Figure S8** online). These data support a major role for *Myd88* signaling in myeloid cell activation during DSS injury.

### *Mlcr* mice contain PSCs that are preferentially distributed near the crypt base

We previously found that in response to DSS treatment, PGE2 produced by the rate limiting enzyme *Ptgs2* acts downstream of *Myd88* in order to maintain colonic epithelial proliferation.<sup>21</sup>

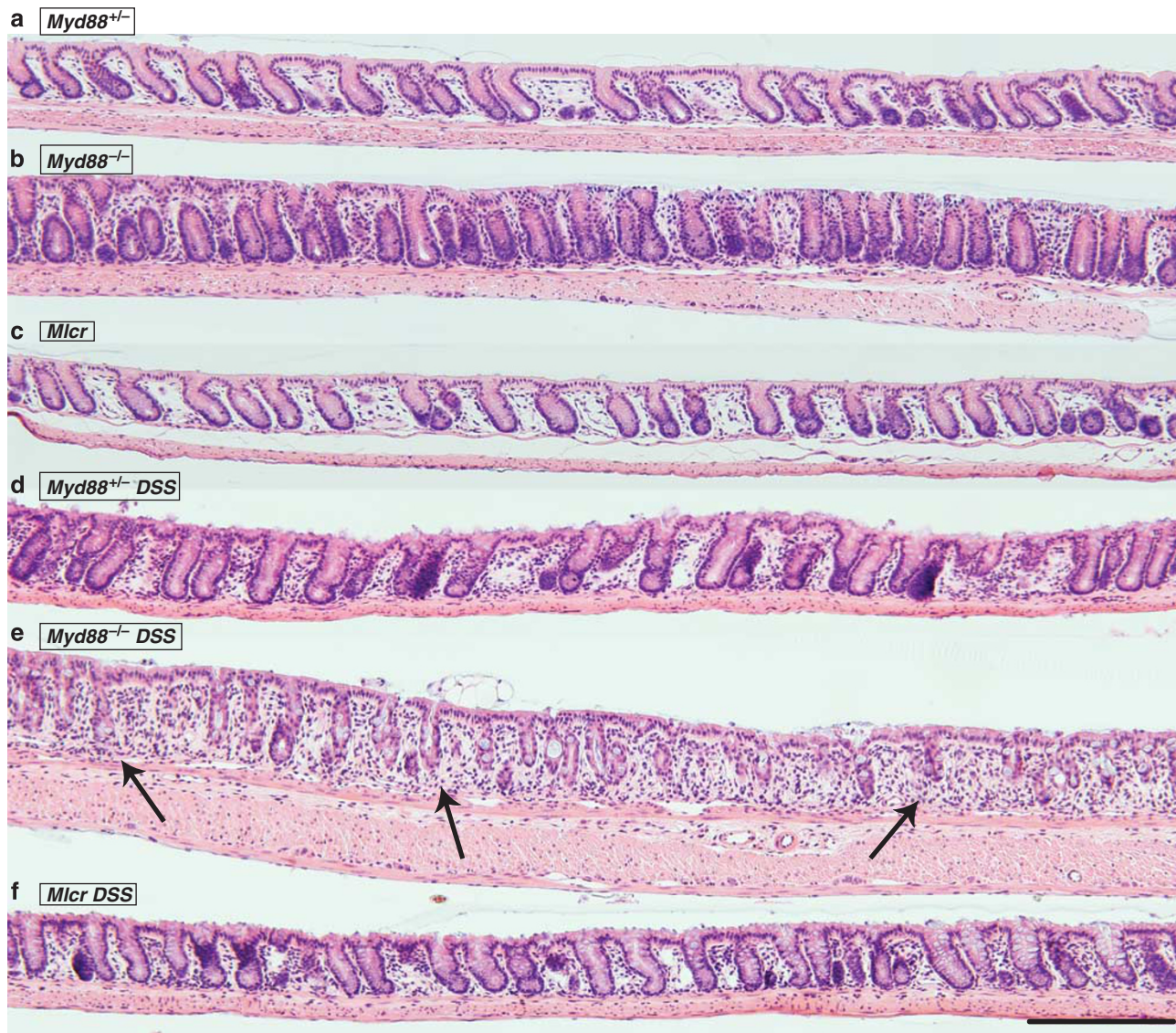


**Figure 4** *Mlcr* mice maintained crypt morphology during dextran sodium sulfate (DSS) treatment. Hematoxylin and eosin-stained sections of descending colons from (a, d) *Myd88*<sup>+/-</sup>, (b, e) *Myd88*<sup>-/-</sup>, and (c, f) *Mlcr* mice. (a–c) Water-treated controls and (d–f) mice treated with 2.5% DSS in drinking water for 7 days. Crypts from DSS-treated *Myd88*<sup>-/-</sup> mice were atrophic (arrows). Descending colonic crypts from DSS-treated *Myd88*<sup>+/-</sup> and *Mlcr* mice were similar in morphology to corresponding untreated mice. Bar = 100 μm.

We also previously established that Ptgs2 expression is readily detectable in mesenchymal stem cells (a.k.a. fibroblasts) both *in vivo* and *in vitro*.<sup>21</sup> Interestingly, it is the distribution of PSCs that is dependent on Myd88 signaling and is associated with maintenance of colonic epithelial proliferation during DSS treatment.<sup>13</sup>

Therefore, we determined the localization of Ptgs2 in tissue sections from DSS-treated and -untreated mice from all three genotypes. In all groups, we observed scattered PSCs that were negative for F4/80 and CD11c antigens (Figure 7a–f). These cells were consistent with fibroblasts by additional marker studies.<sup>13</sup> Quantification of PSCs showed no significant differences in abundance of these cells when comparing groups based on genotype or treatment (Figure 7g), similar to previous

studies.<sup>13</sup> We then determined the levels of Ptgs2 mRNA expression in colonic fibroblasts and colonic myeloid cells isolated from *Mlcr*, *Myd88*<sup>+/-</sup>, and *Myd88*<sup>-/-</sup> mice. For all three genotypes, we found that the expression of Ptgs2 in fibroblasts was significantly higher than myeloid cells (Figure 7h). Additional experiments showed *Myd88*<sup>+/+</sup> also expressed higher levels of Ptgs2 in fibroblasts as compared with myeloid cells (Supplementary Figure S9 online). These findings are consistent with previous studies that show PSCs (fibroblasts) are a prominent source of Ptgs2 in the descending colon in both untreated and DSS-treated mice of multiple genotypes.<sup>13,20</sup>

We previously found that the localization of PSCs was altered in response to DSS treatment in a Myd88-dependent fashion.<sup>13</sup>

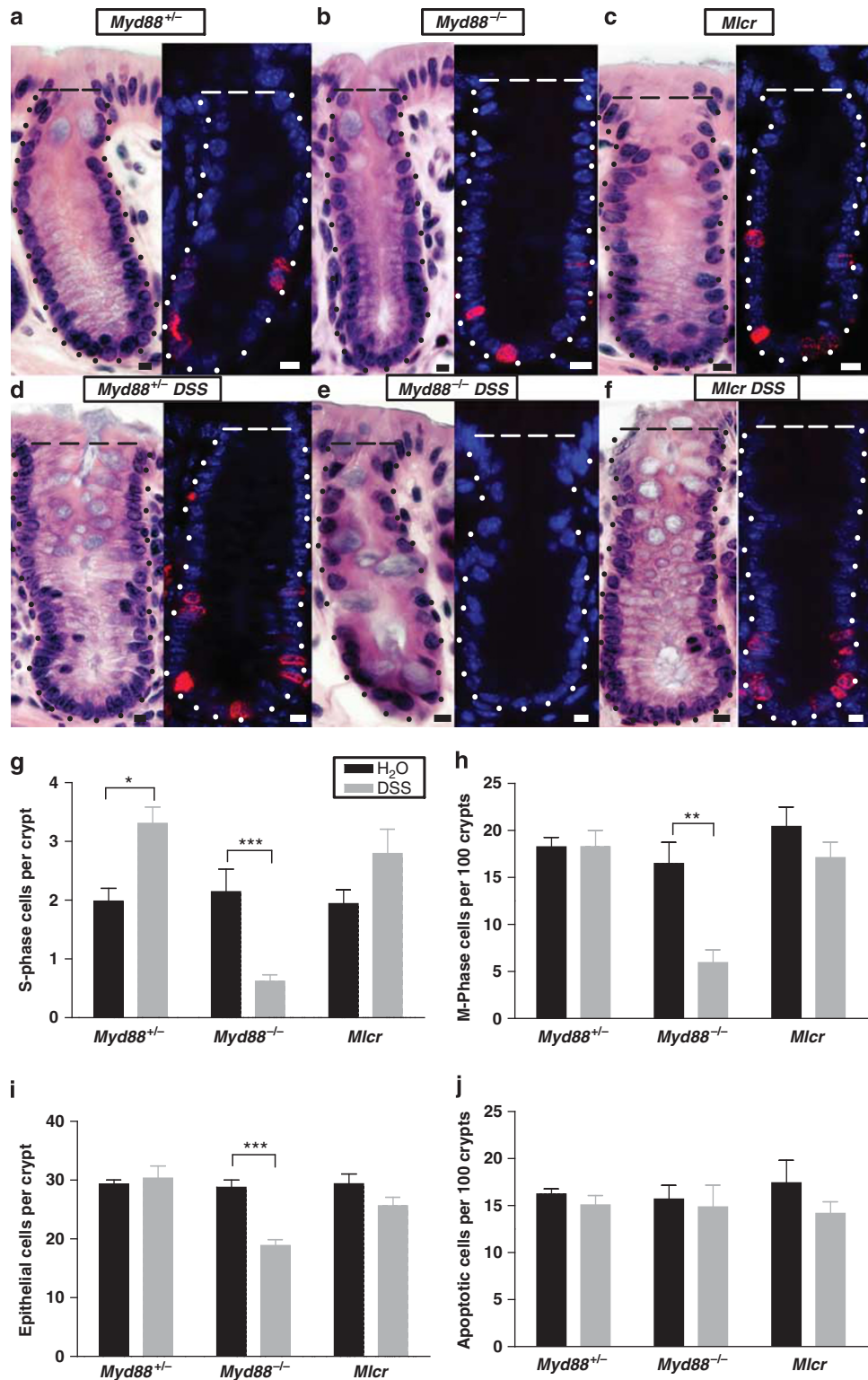


**Figure 5** *Mlcr* mice maintained epithelial proliferation during dextran sodium sulfate (DSS) treatment. Images of descending colonic crypts from (a, d) *Myd88*<sup>+/-</sup>, (b, e) *Myd88*<sup>-/-</sup>, and (c, f) *Mlcr* mice. Images were from mice that were either (a–c) water-treated or (d–f) DSS-treated. Each figure includes sections that were stained with either (left panel) hematoxylin and eosin (H&E) or (right panel) goat-anti-5-bromo-2-deoxyuridine (BrdU) antisera, Alex-Fluor 594-labeled donkey anti-goat IgG (red), and bis-benzamide (blue). The crypt epithelial–mesenchyme junctions (white dotted lines) and the epithelial crypt–surface junctions (white dashed lines) are indicated. Bar = 15  $\mu$ m. Quantification of epithelial proliferation as determined by (g) S-phase (BrdU incorporation) and (h) M-phase analysis. Quantification of (i) crypt cell census and (j) epithelial apoptosis (apoptotic body counts on H&E). Mean values  $\pm$  s.e.m. were plotted for each group ( $N=8$  mice per group analyzed in a total of three separate experiments; 100 well-oriented crypt units analyzed per mouse). Asterisks indicate a statistically significant difference between DSS-treated and corresponding untreated controls (\* $P<0.05$ , \*\* $P<0.01$ , \*\*\* $P<0.001$ ) by one-way analysis of variance and Tukey's post-test.

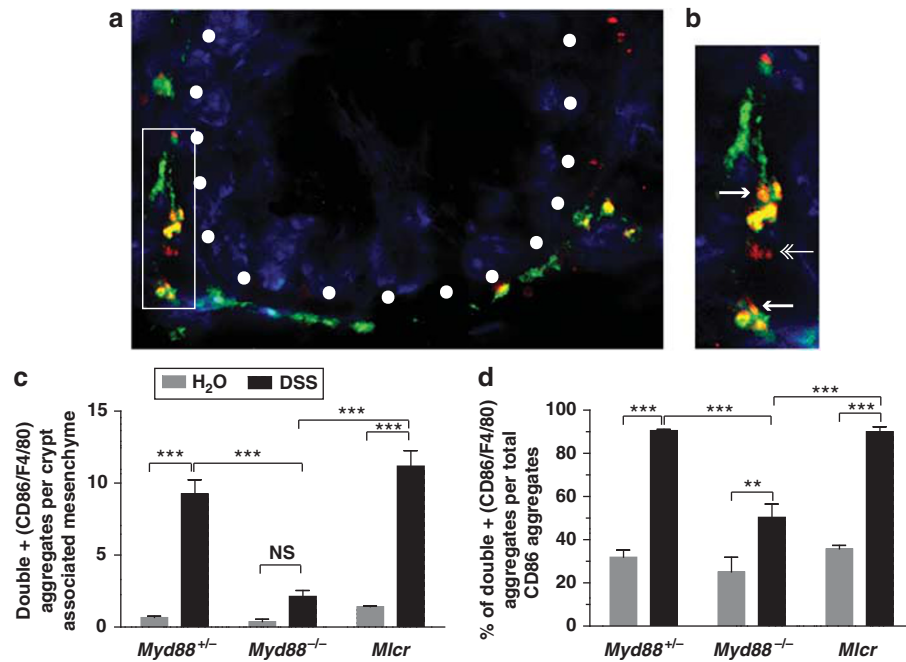


**Figure 6** *Mlcr* macrophages express elevated CD86 during dextran sodium sulfate (DSS) treatment. (a, b) Image of the basal half of a descending colonic crypt and associated mesenchyme from a *Myd88*<sup>+/-</sup> mouse. Sections were stained with rat-anti-mouse CD86 antisera directly conjugated to PerCP (red), rat anti-mouse F4/80 antisera directly conjugated to Alex-Fluor 488 (green), and bis-benzamide (blue). The epithelial–mesenchyme junction is delineated by a white dotted line. Inset in panel a (i.e., (b)) shows CD86-positive aggregates that either co-localized with F4/80 (yellow, arrows) or did not co-localized with F4/80 (red, double head arrow). Bar = 15  $\mu$ m. (c, d) Graph of (c) the number of CD86 aggregates that co-localized with F4/80 per crypt-associated mesenchymal area, and (d) the percentage of CD86 aggregates that co-localized with F4/80. Mean values  $\pm$  s.e.m. were plotted for each group ( $N=4$  mice per group analyzed from two separate experiments;  $N=100$  crypt-associated mesenchyme units were evaluated per mouse). Asterisks indicate statistically significant differences between indicated groups (\*\* $P<0.01$ , \*\*\* $P<0.001$ ) as determined by analysis of variance and Tukey's post-test. NS, not significant.

As anticipated, PSCs were enriched in the peri-crypt base region of DSS-treated *Myd88*<sup>+/-</sup> mice (vs. untreated controls) but were not enriched in this region of DSS-treated *Myd88*<sup>-/-</sup> mice (vs. untreated controls; **Figure 8a** and **b**). As an additional control, we compared the distribution of PSCs in untreated and treated *Myd88*<sup>+/-</sup> vs. untreated and treated *Myd88*<sup>+/+</sup> (that we previously reported)<sup>13</sup> and found no differences. Importantly, DSS-treated *Mlcr* mice contained a similar enrichment of PSCs in the peri-crypt base region (vs. untreated *Mlcr* mice). Thus, expression of Myd88 in myeloid cells was sufficient to alter the distribution of PSCs during DSS injury.

#### Myeloid cells in untreated *Mlcr* mice are in a mildly activated state

An unexpected finding was an enrichment of PSCs in the peri-crypt base region of untreated *Mlcr* mice as compared with untreated *Myd88*<sup>+/-</sup> and *Myd88*<sup>-/-</sup> mice (**Figure 8b**). As the DSS experiments showed that myeloid cell activation was correlated with altered PSC distribution, we reanalyzed the data from **Figure 6c** considering only the untreated groups of mice and found a significantly greater number of double-positive (CD86/F4/80) aggregates in untreated *Mlcr* mice as compared with both untreated control groups (analysis of variance with a Tukey's post-test,  $P<0.01$ ). This finding indicated a mild level of colonic myeloid cell activation in untreated *Mlcr* mice.

We then evaluated mRNA expression of additional markers of myeloid cell activation and found small but significant increases in isolated colonic myeloid cells from untreated *Mlcr* mice as compared with control groups (**Figure 9**; **Supplementary Figure S10** online). This difference was not correlated with an alteration in the expression of anti-inflammatory cytokines in *Mlcr* mice (**Supplementary Figure S11** online). Thus, the myeloid cells in *Mlcr* colons appear to be mildly activated.

As enhanced activation of NF $\kappa$ B in the intestinal epithelium leads to inflammation, fibrosis, and tumorigenesis in aged mice,<sup>39</sup> we evaluated the gross and histological pathology of 12–13-month-old *Mlcr* mice. Interestingly, there was no evidence of inflammation, fibrosis, or tumorigenesis. In contrast, there was a decrease in epithelial proliferation in the transverse colon as compared with littermate controls (**Supplementary Figure S12** online).

#### DISCUSSION

In this study, we determined the role of Myd88 signaling in myeloid-derived cells. We first created a mouse model (*Mlcr*) where Myd88 expression was directed to this lineage using a myeloid-specific Cre and a Myd88 cDNA knocked into the ROSA26 locus. We found this genetic system appropriately restricted Myd88 expression to cell types known to be targeted by *LysM-Cre* and mediated effects in isolated myeloid-derived



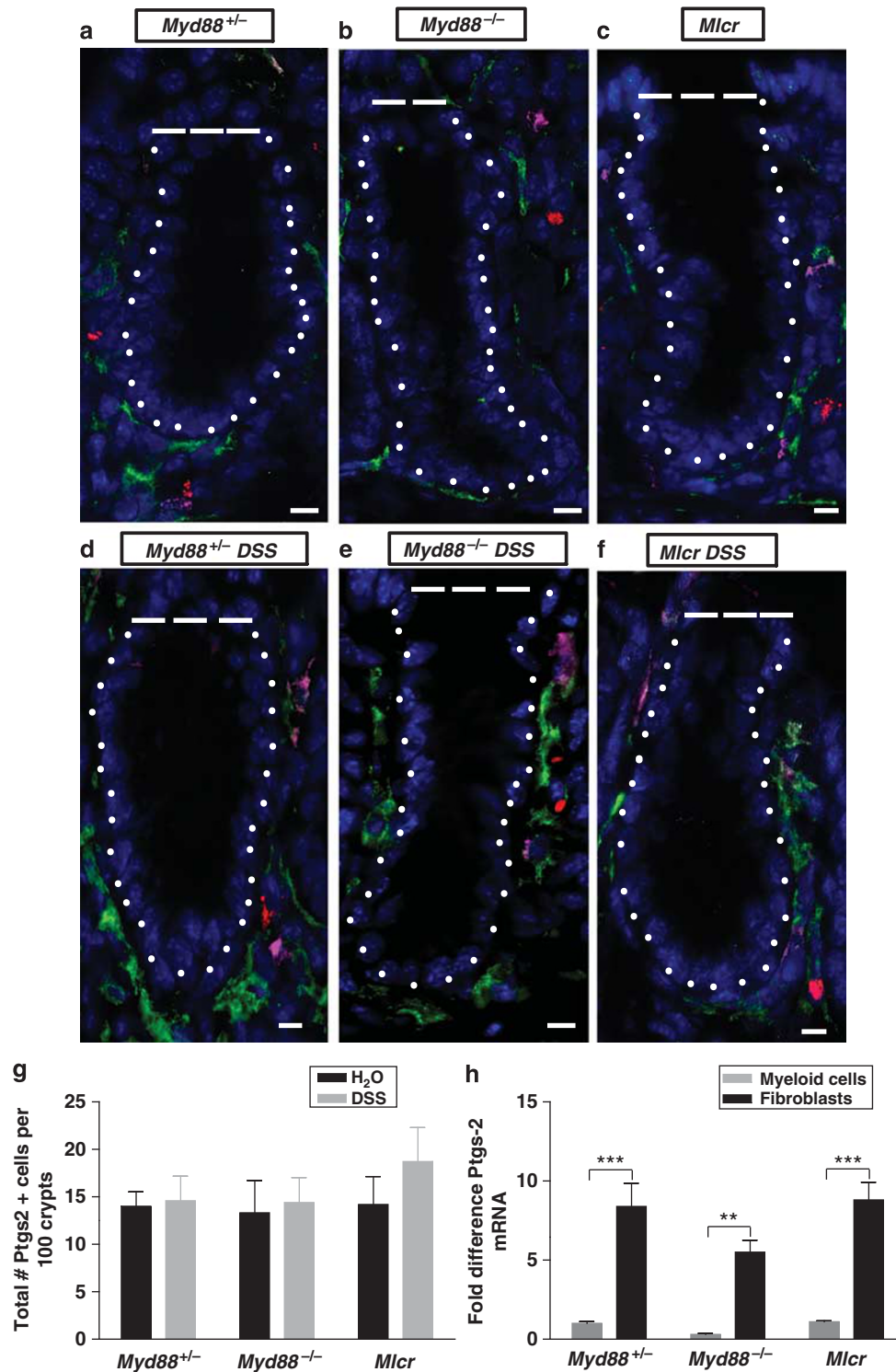


**Figure 7** Colonic fibroblasts express Ptgs2 in *Mlcr* mice. (a–f) Images of descending colonic crypts and surrounding mesenchyme from (a, d) *Myd88*<sup>+/+</sup>, (b, e) *Myd88*<sup>-/-</sup>, and (c, f) *Mlcr* mice. Images from mice that were either (a–c) water-treated or (d–f) dextran sodium sulfate (DSS)-treated. Sections were stained with mouse-anti-Ptgs2 antisera labeled with Alexa-Fluor 594 (red), rat anti-mouse F4/80 antisera directly conjugated to Alexa-Fluor 488 (green), rat anti-mouse CD11c antisera directly conjugated to Alexa-Fluor 647 (pink), and bis-benzamide (blue). The crypt epithelial–mesenchyme junctions (white dotted lines) are indicated. Bars = 15  $\mu$ m. (g) Graph of the number of Ptgs2-positive cells (fibroblasts) per 100 crypt–mesenchyme units for the indicated genotypes and treatments ( $N=6$  mice per group analyzed from two separate experiments;  $N=100$  crypt–mesenchyme units evaluated per mouse). (h) Graph of the relative messenger RNA (mRNA) expression levels of Ptgs2 in isolated colonic fibroblasts and myeloid cells. Y-axis values were a fold difference between the average  $\Delta C_T$  of the experimental cell type and average  $\Delta C_T$  of the control cells (*Myd88*<sup>+/+</sup> myeloid cells) divided by the control  $\Delta C_T$ . Mean values  $\pm$  s.e.m. were plotted for each group ( $N=4$  mice per group analyzed from two separate experiments). Asterisks indicate a statistically significant difference between indicated groups (\*\* $P<0.01$ , \*\*\* $P<0.001$ ) as determined by analysis of variance and Tukey's post-test.

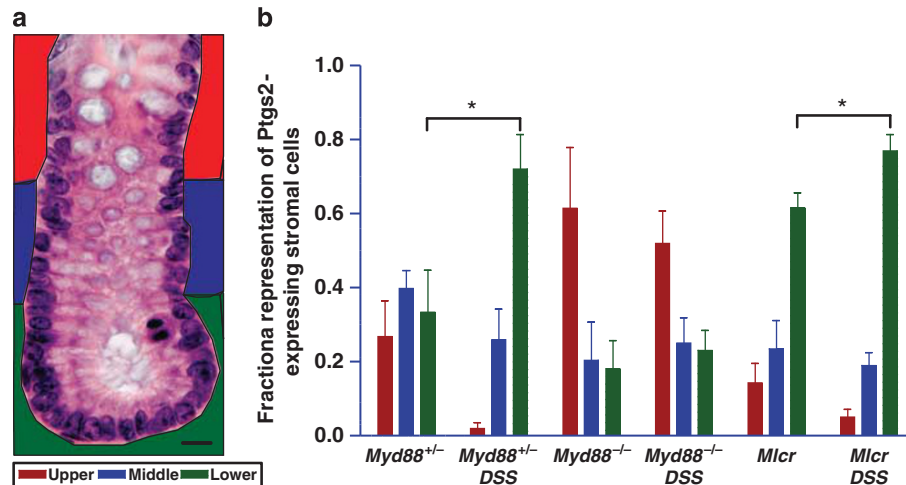


**Figure 8** Ptg2-expressing stromal cells are preferentially distributed in the crypt base-associated mesenchyme of *Mlcr* mice. (a) Map of three mesenchymal zones associated with distinct populations of epithelial cells (Panel a; upper=red, surface, middle=blue, post-mitotic crypt, lower=green, proliferative crypt base). Bar=5  $\mu$ m. (b) Graph of the fractional representation of Ptg2-expressing stromal cells located in each mesenchymal zone for each genotype calculated with and without dextran sodium sulfate (DSS) treatment ( $N=6$  mice per group analyzed from two separate experiments;  $N=100$  crypt-mesenchyme units analyzed per mouse). Asterisks indicate a statistically significant difference in the fractional representation in the lower mesenchyme when comparing treated to untreated for a given genotype ( $*P<0.05$ , Student's *t*-test).

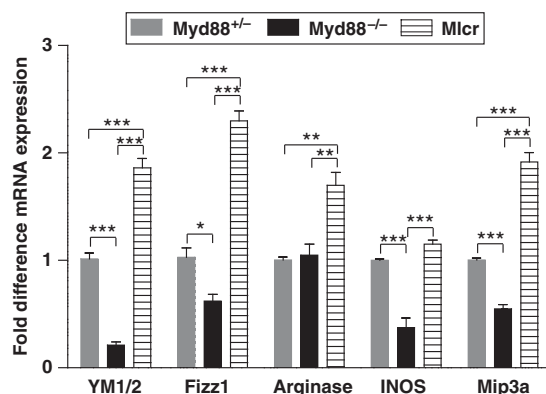


**Figure 9** Untreated *Mlcr* mice contain mildly activated myeloid cells. Graph of the relative messenger RNA (mRNA) expression levels of multiple markers of myeloid cell activation. For each gene, Y-axis values were a fold difference between the average  $\Delta C_T$  of the experimental cell type and average  $\Delta C_T$  of the control cells (*Myd88*<sup>+/-</sup> myeloid cells) divided by the control  $\Delta C_T$ . Mean values $\pm$ s.e.m. were plotted for each group ( $N=4$  mice per group analyzed from two separate experiments). Asterisks indicate a statistically significant difference between indicated groups ( $*P<0.05$ ,  $**P<0.01$ ,  $***P<0.001$ ) as determined by analysis of variance and Tukey's post-test.

cells. Importantly, we showed that restricted expression of Myd88 using *LysM-Cre* was sufficient to rescue the phenotype in *Myd88*<sup>-/-</sup> DSS-injured mice. The colonic features of this mouse model during DSS treatment were comparable to similarly treated *Myd88*<sup>+/-</sup> mice, and included epithelial responses to damage, myeloid cell activation, and localization of PSCs. Interestingly, we found that in uninjured mice, the *Mlcr* line contained mildly activated colonic myeloid cells, indicating that Myd88 signaling in non-myeloid lineages can inhibit myeloid activation.

Myd88 has a role in numerous biological processes within a variety of tissues that include wound repair in lung<sup>40</sup> and skin<sup>41</sup>, cancer<sup>42</sup> and host defense against pathogens.<sup>43</sup> Creation of a floxed allele of this gene by other investigators has been beneficial to determine if deficiency in a particular lineage(s) is required for the function of Myd88 in the whole animal.<sup>44,45</sup> In contrast to a transgenic over-expression approach,<sup>46</sup> we designed our model with the intention to create a flexible genetic system based on breeding to additional Cre lines. In addition, we found that *Mlcr* mice contained levels of Myd88 expression in myeloid cells that was comparable to myeloid cells isolated from *Myd88*<sup>+/-</sup> and *Myd88*<sup>+/+</sup> mice. In contrast to bone marrow chimeras<sup>47,48</sup> where radio-resistant tissue myeloid cells could possibly confound interpretation, our system has the advantage of more precise control of Myd88 expression. We anticipate that our model should complement findings using a floxed Myd88 allele.

We chose *LysM-Cre* to test the role of Myd88 in myeloid cells as this Cre targets macrophages and dendritic cells<sup>27,28</sup> and thus mimics the cell types in the colon that are diminished in mice with *Csfl*-inactivating mutations. Thus, we could evaluate the role of Myd88 expression in comparable cell types. *LysM-Cre* also targets neutrophils.<sup>27,28</sup> Here and in our previous study, we have found no obvious role for neutrophils in the response to DSS injury.<sup>10</sup> In addition, we examined an area of the colon that does not undergo extensive damage during DSS treatment and thus there is no accumulation of neutrophils in this area. For these reasons, we focused our analysis on monocyte-derived cells in *Mlcr* mice.

We previously found a robust, Myd88-dependent, simultaneous elevation of mRNA signatures for both classical and alternative forms of macrophage activation in the mesenchyme of DSS-treated mice.<sup>10</sup> We evaluated the expression of CD86

as it is well recognized as a marker of activated macrophages under both conditions of classical and alternative activation. Elevated CD86 expression in myeloid cells has been reported in a model of spontaneous colitis (*Stat3<sup>fl/fl</sup>;LysM<sup>Cre/+</sup>*).<sup>49</sup> CD86 can be expressed in antigen-presenting cells where it has co-stimulatory properties.<sup>35,38,50</sup> Here, using CD86 as a readout, we found that Myd88 expression in myeloid cells was sufficient to drive myeloid cell activation during DSS treatment.

An unexpected finding was that colonic myeloid cells in untreated *Mlcr* mice showed evidence of mild activation as compared with untreated *Myd88<sup>+/-</sup>* mice. This finding suggests that a source of Myd88 stimulation was unmasked and could include either microbial- or host-derived factors. The finding also suggests the possibility that an additional cellular source of the Myd88 expression may reduce myeloid activation in a non-cell-autonomous manner. This question is of importance as myeloid-derived cells in the intestine are hypoactive in the gut.<sup>2,3</sup> Thus, the *Mlcr* model should be an interesting system to approach this question and determine the interactive roles of Myd88 signaling in multiple lineages of the intestine.

## MATERIALS AND METHODS

**Mice.** The Washington University Medical School Animal Studies Committee approved all animal experiments. Mice were maintained in a specific pathogen-free barrier facility under a strict 12-hour light/dark cycle and fed autoclaved chow diet (B&K Universal, Grimston, Aldbrough, UK). The 6–10-week-old mice were used for experiments. We treated with DSS as previously described.<sup>10,13</sup>

**Generation of *Mlcr* mice.** We subcloned the cDNA for Myd88 into Rosa26PA.<sup>24,25</sup> The linearized targeting vector was electroporated into F1 B6/129SV ES cells. Positive clones were identified by Southern blotting, injected into C57/B6 blastocysts, and implanted into surrogates. Mice with germline transmission were bred to *Myd88<sup>-/-</sup>*,<sup>10,13</sup> and *LysM<sup>Cre/Cre</sup>* mice (Jackson Laboratories, Bar Harbor, ME). All experimental mice were littermates on a mixed C57B6/129SV background.

**Genotyping. *Myd88* locus.** Primers: Myd88 Forward 5'-TGG CAT GCC TCC ATC ATA GTT AAC C-3'; Myd88; Reverse 5'-GTC AGA AAC AAC CACCACAT GC-3'; Myd88 Neo 5'-ATCGCCTTCTATCGCCTTCT T GAC G-3'.

PCR protocol: 5 °C for 2 min; followed by 30 cycles of: 95 °C for 30 s, 60 °C for 30 s, and 72 °C for 30 s; followed by 72 °C for 5 min. PCR products were visualized on 2.75% TBE agarose gels run for 1.5 h at 100 V to clearly separate the amplicons. A 550 base-pair amplicon indicated a wild-type *Myd88* locus and a 600 base-pair amplicon indicated a knock-out *Myd88* locus.

***Mlcr* locus.** Primers: Forward 5'-CCC CAA CGA TAT CGA GTT TG-3'; Reverse 5'-CTT GGT GCA AGG GTT AT-3'.

PCR: 95 °C for 2 min; followed by 35 cycles of: 95 °C for 20 s, 55 °C for 30 s, and 72 °C for 70 s; followed by 72 °C for 5 min. Refer to **Table 2** for interpretation of the three potential amplicons.

***LysM-Cre* locus.** Primers: Forward 5'-AGG TTC GTT CAC TCA TG G A-3'; Reverse 5'-TCG ACC AGT TTA GTT ACC C-3'.

PCR: 95 °C for 2 min; followed by 30 cycles of: 95 °C for 30 s, 60 °C for 30 s, and 72 °C for 30 s; followed by 72 °C for 5 min. A 220 base-pair amplicon indicated presence of Cre in the *LysM* locus.

**Histochemistry and immunohistochemistry.** Colons were dissected, submerged in Bouin's fixative for 4 h at 24 °C or methacarn fixative for 2 h at 24 °C, and embedded in 2% agar for paraffin processing.

**Table 2 Interpretation of *Mlcr* genotyping**

Genotype	746 band	538 band	342 band
<i>MydRosa</i> + <i>Myd88</i> <sup>-/-</sup>	-	-	+
<i>MydRosa</i> - <i>Myd88</i> <sup>-/-</sup>	-	-	-
<i>MydRosa</i> + <i>Myd88</i> <sup>+/-</sup>	+	+	+
<i>MydRosa</i> - <i>Myd88</i> <sup>+/-</sup>	+	-	-
<i>MydRosa</i> + <i>Myd88</i> <sup>+/+</sup>	+	+	+
<i>MydRosa</i> - <i>Myd88</i> <sup>+/+</sup>	+	-	-

PCR product sizes that correspond to each genotype are indicated.

Serial 5- $\mu$ m-thick sections of the descending colons were cut along the cephalocaudal axis and perpendicular to the mucosal surface. Sections were stained with hematoxylin and eosin.<sup>10</sup> For frozen sections, dissected colons were flushed first with phosphate-buffered saline (PBS) followed by OCT media, arranged as 2 cm segments in histology cassettes and frozen with cytocool. Serial 7- $\mu$ m-thick sections of descending colons were cut along the cephalocaudal axis and perpendicular to the mucosal surface.

We performed intraperitoneal injections in mice with a solution containing 5-bromo-2-deoxyuridine (120 mg kg<sup>-1</sup>) and 5'-fluor-2'-deoxyuridine (12 mg ml<sup>-1</sup>; Sigma-Aldrich, St Louis, MO) 1 h before killing. S-phase cells were identified in tissue sections using goat anti-5-bromo-2-deoxyuridine IgG.<sup>10,13</sup>

Ptgs2 localization was performed on 5- $\mu$ m-thick sections of methacarn-fixed tissues stained with mouse IgG1 anti-Ptgs2 mAb (clone 33; BD Biosciences, San Diego, CA; 1:50) and the Zenon antibody labeling system (Invitrogen, Grand Island, NY) as previously described.<sup>13</sup> For co-labeling experiments with Ptgs2, F4/80, and CD11c, 7- $\mu$ m-thick sections of frozen tissue were stained with mouse IgG1 anti-Ptgs2 mAb (clone 33; BD Biosciences; 1:50) and the Zenon antibody labeling system (Invitrogen), rat IgG2b anti-mouse F4/80 mAb directly conjugated to Alexa-488 (clone CI:A3-1; Biolegend, San Diego, CA; 1:100) and Armenian hamster IgG anti-mouse CD11c mAb directly conjugated to Alexa-647 (clone N418; Biolegend; 1:50 O/N 4 °C). Ig isotype controls for all antibodies used for all immunofluorescence studies. Myd88 was detected on frozen, methanol-fixed sections using an overnight incubation of rabbit anti mouse Myd88 antisera (Abcam, Cambridge, MA; 1:750 dilution) followed by tyramide amplification of signal (Invitrogen).

Co-localization of the macrophage activation marker CD86 and F4/80 was performed on 7- $\mu$ m-thick sections of frozen tissue stained with rat IgG2a anti-mouse CD86 mAb directly conjugated to PerCP (clone GL:1; Biolegend; 1:100) and rat IgG2b anti-mouse F4/80 mAb directly conjugated to Alexa-488 (clone CI:A3-1; Biolegend; 1:100). These stained tissue sections were used to analyze CD86 aggregate per crypt base mesenchyme that co-localized with F4/80-positive cells.

**Cell culture media.** Bone marrow-derived macrophage-conditioned media (BM20) consisted of Dulbecco's modified Eagle's medium (DMEM) media supplemented with 10% fetal bovine serum, 20% L-cell supernatant (from L929 fibroblasts), 5% horse serum, 1% L-glutamine, 1% sodium pyruvate, 1:100 of 1 M HEPES, 1  $\mu$ l ml<sup>-1</sup> of 10,000 U ml<sup>-1</sup> penicillin/streptomycin (Abx), with media changed on day 4 and 7. Bone marrow-derived dendritic cells culture media (DC10) was RPMI1640 media supplemented with 10% fetal bovine serum, 1  $\mu$ l ml<sup>-1</sup> of 10,000 U ml<sup>-1</sup> penicillin/streptomycin, 2% L-glutamine, 2% GM-CSF supernatant (B78hi hybridoma), 1% sodium pyruvate, 1% nonessential amino acids, media changed on day 4, 6, and 7.

Fibroblast media consisted of DMEM media supplemented with 10 mM HEPES, 10% fetal bovine serum, and 1  $\mu$ l ml<sup>-1</sup> of 10,000 U ml<sup>-1</sup> penicillin/streptomycin.

Colonic myeloid cell isolation media consisted of DMEM media supplemented with 10 mM HEPES, 1  $\mu\text{M}$  of 10,000 U  $\text{ml}^{-1}$  penicillin/streptomycin, L-glutamate in both DM10 and DM-Abx, and 10% fetal bovine serum in DM10 only.

#### Isolation of fibroblasts and myeloid cells from the colon and macrophages, and dendritic cells derived from bone marrow.

Colonic stromal fibroblasts were isolated from individual mice as previously described.<sup>21</sup> Cells were cultured in supplemented DMEM until confluent, media changed every 3 days.

Bone marrow-derived macrophages and dendritic cells were cultured from bone marrow flushed from the femurs and tibias of a single mouse into 30 ml of DMEM. The cell suspension was split into two equal portions and 35 ml of a specific conditioned media was added to each aliquot. The cell suspensions were then pipetted into 10 $\times$ 15-cm non-tissue culture Petri dishes (5 plates, 10 ml per plate), and the cells were incubated in a standard tissue culture incubator for 7 days to stimulate differentiation into either macrophages (incubated in BM20 media) or dendritic cells (incubated in DC10 media). For LPS experiments, cells were treated with EDTA to remove them from the plate. The cells were then replated at 1.25 $\times$ 10<sup>5</sup> cells per ml for 18 h overnight, and then treated for 1 h with 10 ng  $\text{ml}^{-1}$  LPS from *E. coli* (Sigma-Aldrich) or fresh conditioned media.

Mouse colonic myeloid cells were isolated using a protocol derived from multiple previous studies.<sup>30–32,51–53</sup> Briefly, whole colons were removed, flushed with 1:1 DMEM:PBS, cut into 1 mm pieces using with a sterile razor blade, and the fragments were then placed in a sterile beaker with 40 ml of DM10, 400  $\mu\text{l}$  of 0.5 M EDTA, and 37.7  $\mu\text{l}$  of 1 M dithiothreitol. The suspension was placed in an orbital shaker (250 r.p.m.) for 20 min at 37°C and then filtered using a 100  $\mu\text{m}$  cell filter (Fisher, Pittsburgh, PA). The tissue fragments were washed three times with shaking in DM-Abx supplemented with 400  $\mu\text{l}$  of 0.5 M EDTA and filtered after each wash. The washed tissue fragments were further minced with sterile razor blade and the fragments were placed in 15 ml of DM-Abx supplemented with 475  $\mu\text{l}$  of 5 mg  $\text{ml}^{-1}$  collagenase IV and 150  $\mu\text{l}$  of 10 mg  $\text{ml}^{-1}$  DNase. The suspension was placed in an orbital shaker (250 r.p.m.) for 30 min at 37°C. The suspension was then passed through a 70  $\mu\text{m}$  cell filter. The media were retained and 15 ml of DM10 supplemented with 150  $\mu\text{l}$  of DNase (10 mg  $\text{ml}^{-1}$ ) was added. The suspension was centrifuged at 1,200  $g$  for 5 min at 24°C. The media was carefully removed and the cell pellet was resuspended in 12 ml of DM10. The cells were then plated in a non-tissue culture-treated Petri dish for 1 h. The adherent cells were washed three times with sterile PBS. The cells were then treated with 5 ml of EDTA/PBS and incubated at 4°C for 10 min. The plate was scraped to remove adherent cells. The cells were resuspended in 5 ml of DM10 and 5 ml of EDTA/PBS, and centrifuged at 1,200  $g$  for 5 min to pellet the myeloid cells.

**RNA extraction and quantitative real-time PCR analysis.** RNA was extracted using NucleoSpin RNA II (Clontech Laboratories, Mountain View, CA) for colonic fibroblasts and bone marrow-derived macrophages and dendritic cells. Colonic myeloid cell RNA was isolated using the PicoPure RNA Isolation Kit (Applied Biosystems, Carlsbad, CA). The quality and quantity of all RNAs were evaluated by Nanodrop (Thermo Scientific, Waltham, MA). Random primed cDNA (Superscript III, Invitrogen) was used as a template for quantitative real-time PCR that was performed in triplicate for each biologic sample using SYBR Advantage (Clontech, Mountain View, CA). The threshold cycle ( $C_T$ ) of the gene of interest was subtracted from the baseline  $C_T$  (18s mRNA) to calculate a change in  $C_T$  ( $\Delta C_T$ ). To calculate the fold change in gene expression, the  $\Delta C_T$  for each measurement was subtracted from the baseline  $\Delta C_T$  (average  $\Delta C_T$  of *Myd88*<sup>+/-</sup> untreated cells mRNA).

**Primers used for qPCR.** 18S (5'-CATTCGAACGTCTGCCCTATC-3' and 5'-CCTGTGCCTTCCTTGGA-3'), *Ptgs2* (5'-TGCCTGGTC TGATGATGATG-3' and 5'-GGGGTGCCAGTGATAGAGTG-3'),

TNF- $\alpha$  (5'-CCCTCACACTCAGATCATCTTCT-3' and 5'-GCTACGACGTGGGCTACAG-3'), and *Myd88* (5'-CACCTG TGTCTGGTCCATTG-3' and 5'-CTGTTGGACCTGGAGACA-3'). The latter primers were designed to include exons 4 and 5 so as to amplify only intact mRNA as found in *Myd88*<sup>+/-</sup> but not *Myd88*<sup>-/-</sup> mice.

**SUPPLEMENTARY MATERIAL** is linked to the online version of the paper at <http://www.nature.com/mi>

#### ACKNOWLEDGMENTS

We thank E Unanue, W Stenson, N Manieri, and M Walker for comments on the manuscript, and M White for microinjection of targeted ES cells. This work was supported by the National Institutes of Health (DK071619), Crohn's Colitis Foundation of America, Pew Scholars Foundation, and Washington University Digestive Disease Research Core (NIH P30-DK52574).

#### DISCLOSURE

The authors declared no conflict of interest.

© 2012 Society for Mucosal Immunology

#### REFERENCES

- Ley, R.E., Peterson, D.A. & Gordon, J.I. Ecological and evolutionary forces shaping microbial diversity in the human intestine. *Cell* **124**, 837–848 (2006).
- Hill, D.A. & Artis, D. Intestinal bacteria and the regulation of immune cell homeostasis. *Annu. Rev. Immunol.* **28**, 623–667 (2010).
- Hooper, L.V. & Macpherson, A.J. Immune adaptations that maintain homeostasis with the intestinal microbiota. *Nat. Rev. Immunol.* **10**, 159–169 (2010).
- Abreu, M.T. Toll-like receptor signalling in the intestinal epithelium: how bacterial recognition shapes intestinal function. *Nat. Rev. Immunol.* **10**, 131–144 (2010).
- Chang, W.W. & Leblond, C.P. Renewal of the epithelium in the descending colon of the mouse. *Am. J. Anat.* **131**, 73–99 (1971).
- Li, L. & Clevers, H. Coexistence of quiescent and active adult stem cells in mammals. *Science* **327**, 542–545 (2010).
- Walker, M.R., Patel, K.K. & Stappenbeck, T.S. The stem cell niche. *J. Pathol.* **217**, 169–180 (2008).
- Seno, H., Miyoshi, H., Brown, S.L., Geske, M.J., Colonna, M. & Stappenbeck, T.S. Efficient colonic mucosal wound repair requires Trem-2 signaling. *Proc. Natl. Acad. Sci. USA* **106**, 256–261 (2009).
- Stappenbeck, T.S. & Miyoshi, H. The role of stromal stem cells in tissue regeneration and wound repair. *Science* **324**, 1666–1669 (2009).
- Pull, S.L., Doherty, J.M., Mills, J.C., Gordon, J.I. & Stappenbeck, T.S. Activated macrophages are an adaptive element of the colonic epithelial progenitor niche necessary for regenerative responses to injury. *Proc. Natl. Acad. Sci. USA* **102**, 99–104 (2005).
- Ghia, J., Galeazzi, F., Ford, D.C., Hogaboam, C.M., Vallance, B.A. & Collins, S. Role of M-CSF-dependent macrophages in colitis is driven by the nature of the inflammatory stimulus. *Am. J. Physiol. Gastrointest. Liver Physiol.* **294**, G770–G777 (2008).
- Lucas, T. *et al.* Differential roles of macrophages in diverse phases of skin repair. *J. Immunol.* **184**, 3964–3977 (2010).
- Brown, S. *et al.* *Myd88*-dependent positioning of *Ptgs2*-expressing stromal cells maintains colonic epithelial proliferation during injury. *J. Clin. Invest.* **117**, 258–269 (2007).
- Rakoff-Nahoum, S., Paglino, J., Eslami-Varzaneh, J., Edberg, S. & Medzhitov, R. Recognition of commensal microflora by Toll-Like receptors is required for intestinal homeostasis. *Cell* **118**, 229–241 (2004).
- Medzhitov, R. *et al.* *MyD88* is an adaptor protein in the hToll/IL-1 receptor family signaling pathways. *Mol. Cell* **2**, 253–258 (1998).
- Schnare, M., Barton, G.M., Holt, A.C., Takeda, K., Akira, S. & Medzhitov, R. Toll-like receptors control activation of adaptive immune responses. *Nat. Immunol.* **2**, 947–950 (2001).
- Otte, J., Rosenberg, I.M. & Podolsky, D.K. Intestinal myofibroblasts in innate immune responses of the intestine. *Gastroenterology* **124**, 1866–1878 (2003).

18. Vamadevan, A.S., Fukata, M., Arnold, E.T., Thomas, L.S., Hsu, D. & Abreu, M.T. Regulation of Toll-like receptor 4-associated MD-2 in intestinal epithelial cells: a comprehensive analysis. *Innate Immun.* **16**, 93–103 (2010).
19. Wang, D., Mann, J.R. & DuBois, R.N. The role of prostaglandins and other eicosanoids in the gastrointestinal tract. *Gastroenterology* **128**, 1445–1461 (2005).
20. Sonoshita, M., Takaku, K., Oshima, M., Sigihara, K. & Taketo, M. Cyclooxygenase2 expression in fibroblasts and endothelial cell of intestinal polyps. *Can. Res.* **62**, 6846–6849 (2002).
21. Walker, M.R., Brown, S.L., Riehl, T.E., Stenson, W.F. & Stappenbeck, T.S. Growth factor regulation of prostaglandin-endoperoxide synthase 2 (Ptgs2) expression in colonic mesenchymal stem cells. *J. Biol. Chem.* **285**, 5026–5039 (2009).
22. Nomura, T., Chang, H.Y., Lu, R., Hankin, J., Murphy, R.C. & Schuster, V.L. Prostaglandin signaling in the renal collecting duct. *J. Biol. Chem.* **280**, 28424–28429 (2005).
23. Koch, S. *et al.* The wnt antagonist dkk1 regulates intestinal epithelial homeostasis and wound repair. *Gastroenterology* **141**, 259–268 (2011).
24. Srinivas, S., Watanabe, T., Lin, C., William, C.M., Tanabe, Y., Jessell, T.M. & Constantini, F. Cre reporter strains produced by targeted insertion of *EYFP* and *ECFP* into the *ROSA26* locus. *BMC Dev. Biol.* **1**, 1471–1478 (2001).
25. Lavine, K., Schmid, G., Smith, C. & Ornitz, D. Novel tool to suppress cell proliferation *in vivo* demonstrates that myocardial and coronary vascular growth represent distinct developmental programs. *Dev. Dyn.* **237**, 713–724 (2008).
26. Soriano, P. Generalized *lacZ* expression with the *ROSA26* Cre reporter strain. *Nat. Gen.* **21**, 70–71 (1999).
27. Cross, M., Mangelsdorf, I., Wedel, A. & Renkawitz, R. Mouse lysozyme M gene: isolation, characterization, and expression studies. *Proc. Natl. Acad. Sci. USA* **85**, 6232–6236 (1988).
28. Clausen, B.E., Burkhardt, C., Reith, W., Renkaritz, R. & Forster, I. Conditional gene targeting in macrophages and granulocytes using *LysMcre* mice. *Transgenic Res.* **8**, 265–277 (1999).
29. Adachi, O. *et al.* Targeted disruption of the *MyD88* gene results in loss of IL-1- and IL-18-mediated function. *Immunity* **9**, 143–150 (1998).
30. Davies, J.Q. & Gordon, S. Isolation and culture of murine macrophages. In: *Methods in Molecular Biology, Vol 290, Basic Cell Culture Protocols* 3rd edn (Helgason, C.D. & Miller, C.L., eds). 91–103 (Humana Press, Totowa, NJ, 2004).
31. Peiser, L., Gordon, S. & Haworth, R. Isolation and measuring the function of professional phagocytes, murine macrophages. In: *Methods in Microbiology, Vol. 32, Immunology of Infection* 2nd edn (D. Kabelitz, ed). 331–335 (Academic Press Science: London, 2002).
32. Ozaki, H. *et al.* Isolation and characterization of resident macrophages from the smooth muscle layers of murine small intestine. *Neurogastroenterol. Motil.* **16**, 39–51 (2004).
33. Kumagai, K., Itoh, K., Hinuma, S. & Tada, M. Pretreatment of plastic petri dishes with fetal calf serum. A simple method for macrophage isolation. *J. Immunol. Methods* **29**, 17–25 (1979).
34. Zanzinger, K., Schellack, C., Nausch, N. & Cerwenka, A. Regulation of triggering receptor expressed on myeloid cells 1 expression on mouse inflammatory monocytes. *Immunology* **128**, 185–195 (2009).
35. Hathcock, K.S., Laszlo, G., Pucillo, C., Linsley, P. & Hodes, R.J. Comparative analysis of B7-1 and B7-2 costimulatory ligands: expression and function. *J. Exp. Med.* **180**, 631–640 (1994).
36. Mosser, D.M. The many faces of macrophage activation. *J. Leukocyte Biol.* **73**, 209–212 (2003).
37. Edwards, J.P., Zhang, X., Frauwrith, K.A. & Mosser, D.M. Biochemical and functional characterization of three activated macrophage populations. *J. Leukocyte Biol.* **80**, 1298–1307 (2006).
38. Nolan, A. *et al.* Differential role for CD80 and CD86 in regulation of the innate immune response in murine polymicrobial sepsis. *PLoS One* **4**, e6600 (2009).
39. Vlantis, K. *et al.* Constitutive IKK2 activation in intestinal epithelial cells induces intestinal tumors in mice. *J. Clin. Invest.* **121**, 2781–2793 (2011).
40. Jiang, D. *et al.* Regulation of lung injury and repair by Toll-like receptors and hyaluronan. *Nat. Med.* **11**, 1173–1179 (2005).
41. Macedo, L., Pinhal-Enfield, G., Alshits, V., Elson, G., Cronstein, B.N. & Leibovich, S.J. Wound healing is impaired in *MyD88*-deficient mice: a role for *MyD88* in the regulation of wound healing by adenosine A2A receptors. *Am. J. Pathol.* **171**, 1774–1788 (2007).
42. Rakoff-Nahoum, S. & Medzhitov, R. Toll-like receptors and cancer. *Nat. Rev. Cancer* **9**, 57–63 (2009).
43. Gibson, D.L., Ma, C., Bergstrom, K.S., Huang, J.T., Man, C. & Vallance, B.A. *MyD88* signaling plays a critical role in host defense by controlling pathogen burden and promoting epithelial cell homeostasis during *Citrobacter rodentium*-induced colitis. *Cell Microbiol.* **10**, 618–631 (2008).
44. Hou, B., Reizis, B. & DeFranco, A.L. Toll-like receptors activate innate and adaptive immunity by using dendritic cell-intrinsic and -extrinsic mechanisms. *Immunity* **29**, 272–282 (2008).
45. Kleinriders, A. *et al.* *MyD88* signaling in the CNS is required for development of fatty acid-induced leptin resistance and diet-induced obesity. *Cell Metab.* **10**, 249–259 (2009).
46. Vaishnav, S., Behrendt, C., Ismail, A., Eckmann, L. & Hooper, L. Paneth cells directly sense gut commensals and maintain homeostasis at the intestinal host-microbial interface. *Proc. Natl. Acad. Sci. USA* **105**, 20858–20863 (2008).
47. Asquith, M.J., Boulard, O., Powrie, F. & Maloy, K.J. Pathogenic and protective roles of *MyD88* in leukocytes and epithelial cells in mouse models of inflammatory bowel disease. *Gastroenterology* **139**, 519–529 (2010).
48. Brandl, K. *et al.* *MyD88* signaling in nonhematopoietic cells protects mice against induced colitis by regulating specific EGF receptor ligands. *Proc. Natl. Acad. Sci. USA* **107**, 19967–19972 (2010).
49. Reindl, W., Weiss, S., Lehr, H.A. & Förster, I. Essential crosstalk between myeloid and lymphoid cells for development of chronic colitis in myeloid-specific signal transducer and activator of transcription 3-deficient mice. *Immunology* **120**, 19–27 (2006).
50. Podjil, J., Kin, N.W. & Sanders, V.M. CD86 and  $\beta$ 2-adrenergic receptor signaling pathways, respectively, increase Oct-2 and OCA-B expression and binding to the 3-IgH enhancer in B Cells. *J. Biol. Chem.* **279**, 23394–23404 (2004).
51. Bull, D.M. & Bookman, M. A. Isolation and functional characterization of human intestinal mucosal lymphoid cells. *J. Clin. Invest.* **59**, 966–974 (1977).
52. Rogler, M. *et al.* Isolation and phenotypic characterization of colonic macrophages. *Clin. Exp. Immunol.* **112**, 205–215 (1997).
53. Schenk, M., Bouchon, A., Birrer, S., Colonna, M. & Mueller, C. Macrophages expressing triggering receptor expressed on myeloid cells-1 are underrepresented in the human intestine. *J. Immunol.* **174**, 517–524 (2005).